

Large magnonic band gaps and spectra evolution in three-dimensional magnonic crystals based on magnetoferritin nanoparticles

S. Mamica,* M. Krawczyk, M. L. Sokolovskyy, and J. Romero-Vivas

Nanomaterials Physics Division, Faculty of Physics, Adam Mickiewicz University in Poznań, ul. Umultowska 85, 61-614 Poznań, Poland

(Received 28 March 2012; revised manuscript received 17 September 2012; published 4 October 2012)

We study magnonic crystals based on magnetoferritin nanoparticles. These nanoparticles self-assemble to form crystals of highly ordered fcc structure with a lattice constant of ten-odd nanometers. Filling the interparticle space by a ferromagnetic material should stabilize the ferromagnetic order in such a crystal at room temperature. We use the plane wave method to demonstrate that the introduction of a ferromagnetic matrix can also lead to the opening of a complete band gap, referred to as a magnonic band gap, in the spin-wave spectrum. We use a model based on a homogeneous medium with effective parameters to interpret the characteristics of the obtained spin-wave spectra in the long wave limit. We also study in detail the width of the band gap and its central frequency versus the matrix material and the lattice constant. The occurrence of a maximum width in the lattice-constant dependence is shown to be closely related to the specific behavior of the dynamic magnetization profiles of the lowest excitations in the spin-wave spectrum. On the basis of our results we determine the conditions conducive to the occurrence of a complete magnonic band gap. We also show that the crystallographic structure and the lattice constant of the crystals produced by the protein crystallization technique are almost optimized for the occurrence of a magnonic band gap.

DOI: [10.1103/PhysRevB.86.144402](https://doi.org/10.1103/PhysRevB.86.144402)

PACS number(s): 75.30.Ds, 75.75.-c, 75.50.Tt, 87.85.jf

I. INTRODUCTION

Magnetic nanoparticles (NPs) have been intensively studied because of their unusual physical properties as well as promising applications, and the interest in them continues to grow.¹ This is due to their potential applications in a wide variety of fields that range from medicine to nanoelectronics.² Biomimetic nanoparticles, a class of NPs grown by biomineralization in biological protein cages, prove to be of use in many fields: As magnetic resonance imaging contrast agents³ or drug delivery vessels,⁴ in the production of nanodot floating gate memory⁵ or new types of battery electrodes,⁶ or for carbon nanotube growth.⁷ Biomimetic NPs are also used in the realization of two-dimensional (2D) and three-dimensional (3D) systems of highly ordered structure.^{8–12} In this study we consider the use of NPs of the very numerous magnetoferritin superfamily¹³ as the basis for the realization of 3D magnonic crystals in which the interparticle space is filled with a ferromagnetic material.

The use of protein cages as reaction chambers for the production of NPs has a number of advantages. One of them is a high level of homogeneity of the NPs in terms of size and shape, determined by the internal surface of the protein cage. The diameter of the biomimetic magnetic nanoparticles ranges from 5 nm for Dps (DNA-binding protein from starved cells)^{14,15} to approximately 100 nm for equine herpesvirus.^{16,17} For a survey of biological particles used as supramolecular templates to encapsulate NPs see, for example, 18 or 19. Another major advantage of biomimetic NPs from the point of view of this study is the possibility of producing highly ordered 3D structures by self-assembly. Moreover, the self-assembly processes depend on the external surface of the protein cage, the characteristics of which can be modified without affecting those of the internal surface, involved in the biomineralization process.²⁰ This allows us to control the self-assembly of biomimetic particles without modifying the core obtained inside the protein cage.

A large class of biomimetic NPs are based on ferritin, a protein that stores iron in a nontoxic form in living organisms.²¹ Ferritin consists of 24 protein subunits forming a spherical cage that can store approximately 4500 Fe atoms. Iron is stored in the form of ferrihydrite (hydrous ferric oxyhydroxide); its removal is the first step in the production of biomimetic NPs. An empty ferritin shell, or apoferritin, is filled with the accumulated material^{22–24} (see, e.g., Refs. 2, 19, or 20 for the wide spectrum of filling materials). If the core obtained in this way has a significant total magnetic moment the nanoparticle is referred to as magnetoferritin (mFT).²⁵ Current technologies allow the production of mFT NPs highly monodisperse in terms of both size and magnetic parameters; for example, with apoferritin completely filled with magnetite/maghemite ($\text{Fe}_3\text{O}_4/\gamma\text{-Fe}_2\text{O}_3$), a commonly used magnetic filling material, the obtained magnetic core has a diameter of approximately 8 nm and a total magnetic moment of the order of $10^4 \mu_B$.^{9,26–28}

The protein crystallization technique has been successfully used for the production of 3D fcc mFT crystals⁹ of highly ordered structure and the external size up to 100 μm . An interesting effect observed in structures produced in this way is a substantial reduction of the lattice constant as a result of dehydration. As prepared, the mFT crystals have a lattice constant of approximately 18.5 nm, which decreases to approximately 14 nm when the crystals are taken off the mother liquor and dried.²⁷ In combination with the possibility of modifying the external surface of mFT NPs this property opens the prospect of controlling the lattice constant with a control range of at least ten-odd nanometers. As demonstrated by our results, even slight changes in the lattice constant in the considered range will modify drastically the spin-wave spectrum of the magnonic crystal.

Magnonic crystals (MCs) are the magnetic counterpart of semiconductor, photonic, and phononic crystals, with spin waves acting as information carriers and thus playing the

same role as electrons and electromagnetic and elastic waves, respectively, in the other three types of crystals.^{29–32} By adjusting the constituent materials, the shape of individual elements and their periodic spatial (or planar) arrangement the dispersion of spin waves in MCs can be tailored in a way impossible in other materials and composites. This implies a possibility of modeling the velocity and direction of the spin waves propagating in the MCs. However, the fundamental characteristic of periodic structures, including magnonic crystals, is the occurrence of a band gap in their energy spectrum. In MCs this band gap is referred to as magnonic band gap, and represents a frequency range unavailable to spin waves propagating in the MC. Along with the possibility of tuning this forbidden frequency range by controlling the applied magnetic field, this property makes MCs the basic building blocks of the new branch of physics referred to as magnonics.^{32–35} The main objective of magnonics is practical application of spin waves for the construction of new logic systems and improvement of parameters and functionalities of rf devices.^{36–41}

The current experimental studies of spin waves in MCs mainly focus on 1D or 2D structures. These tend to be regular lattices of holes (with a period down to a few hundred nanometers) drilled in a homogeneous ferromagnetic material, referred to as antidot lattices,^{42–45} or periodic lattices of stripes or magnetic dots.^{46–49} So far, the occurrence of a magnonic band gap has been verified experimentally in a thin-film one-dimensional (1D) MC composed of two ferromagnetic materials^{50,51} and just recently in a two-component thin-film 2D MC in the form of an antidot lattice in Py with holes filled with Co.⁵² The realization of MCs with a lattice constant of tens of nanometers, though technologically possible, remains a challenge. Magnonic crystals with even smaller lattice constants, down to ten-odd nanometers, have only been studied theoretically so far.^{53,54} Neither have 3D MCs been realized experimentally, and remain the subject of theoretical studies.^{54–58} The protein crystallization technique discussed above seems to open the prospect of realizing 3D MCs with a lattice constant of ten-odd nanometers. This would be an enormous step forward in magnonics, and would allow us to shift the magnonic band gap to the subterahertz frequency range.

A number of methods are used for calculating the spectrum of spin waves in 2D MCs. The calculation techniques include the plane wave method (PWM),^{29,53,59} averaging methods,^{60,61} the dynamical matrix method,^{62–64} and approximative semianalytic techniques.^{65,66} The introduction of periodic boundary conditions to micromagnetic calculations has allowed numerical simulations of spin waves propagating in magnonic systems.^{67–69} Based on the finite difference method or the finite element method, such micromagnetic simulations require, however, huge computer resources and therefore are currently used mainly for studying thin films.^{70,71} Especially PWM seems to be very useful for the theoretical study of the structures considered in this paper. Because of its conceptual simplicity and applicability to any type of lattice and any shape of scattering centers the PWM is one of the most popular tools used for studying MCs as well as photonic and phononic crystals.^{72–75} The method is being constantly improved, its field of application extending

to new problems. Recently, the PWM has been used for calculating the band structure of photonic and magnonic crystals composed of materials with energy dissipation or with frequency-dependent properties,^{76,77} 1D and 2D MCs of finite thickness,^{78,79} 2D antidot lattices,^{80,81} and 2D MCs with a point defect.⁸²

The extension of the PWM to 3D MCs is developed in Refs. 55–58. These papers present a systematic study of the effect of a number of factors on the magnonic band structure; the considered factors include structural parameters (filling fraction, lattice constant, ellipsoidal deformation of the scattering centers) and magnetic properties of the constituent materials (contrast of saturation magnetization and exchange constant). The investigated 3D MCs have the simple cubic (sc),⁵⁵ body-centered cubic (bcc),^{56,57} face-centered cubic (fcc),⁵⁷ and simple hexagonal (sh)⁵⁸ crystallographic structure. Both magnetic contrasts, that is, the saturation magnetization contrast and the exchange constant contrast, are shown to play an important role in the opening of magnonic gaps. A saturation magnetization contrast above a certain critical level provides a sufficient condition for magnonic gaps to open (even if the values of the exchange constant in the constituent materials are equal); the critical value of saturation magnetization contrast strongly depends on the lattice type. The exchange contrast has a significant effect on the gap width, but needs to be very large to induce the opening of magnonic band gaps in the absence of magnetization contrast. As demonstrated in Ref. 57, an important role in the creation of magnonic band gaps is played by the crystallographic structure. The best conditions for the occurrence of magnonic band gaps are offered by the fcc lattice. Moreover, the results of these calculations indicate that the gap width depends on the shape of the scattering centers; in the fcc and bcc structures the largest band gaps are observed for scattering centers with a shape close to a sphere. The important role of the lattice constant is demonstrated in cubic magnonic structures, in which, for lattice constants greater than the exchange length in the matrix material, the dipolar interactions gain in importance, which results in a substantial reduction of the gap width.

The concept of 3D MC was also used in an attempt to explain the experimental data obtained in low-doped manganites by neutron scattering on SWs and proving the occurrence of a spin-wave frequency gap.⁸³ According to a hypothesis proposed in Ref. 56, two phases related with two forms of manganese might self-arrange into a regular bcc lattice of ellipsoidal droplets rich in Mn⁴⁺ immersed in a canted-antiferromagnetic Mn²⁺ matrix. The results based on this model are in good agreement with the experimental SW spectra. The theoretical hypothesis of separate phases forming a regular lattice has not yet been confirmed experimentally, though. In the latest paper⁵⁸ the theoretical considerations are extended to sh lattice-based MCs composed of two ferromagnetic metals. Twelve MCs of different material composition are investigated by considering the combinations of four metallic ferromagnetic materials: Co, Fe, Ni, and Py. The absolute magnonic gap is only found to occur in the MC with Ni spheres in an Fe matrix. The results presented in this reference paper point out the difficulties encountered in the engineering of 3D MCs with a complete band gap from ferromagnetic metals.

In the present paper we propose an MC based on a 3D mFT crystal with a ferromagnetic material used as a matrix. We present the results of numerical calculations of the magnonic band structure for the fcc lattice, a structure characteristic of mFT crystals, in the lattice constant range in which magnetoferritins can aggregate in the protein crystallization process. Five representative ferromagnetic materials are considered, with fixed size and properties of mFT NPs. We show that a complete magnonic gap should open with a suitably chosen matrix material, and provide a qualitative explanation of this effect. Moreover, our analysis of the impact of the lattice constant of the MC on the properties of the magnonic band gap leads to the conclusion that the natural separation of mFT NPs is close to the optimal value for which the obtained complete, or omnidirectional, magnonic gap is the largest. We use an adaptation of the PWM suitable for the treatment of 3D MCs, in the development of which we extend the model presented in previous papers devoted to 3D MCs (Refs. 55–58) by taking into account the effect of inhomogeneous static demagnetizing field. Each of these four papers presents a detailed study of the effect of the structural and material parameters on the width of the magnonic band gap, but does not elucidate its physical origin. Here we clarify this issue with the aid of the empty lattice approach. We also readdress the problem of reduction of the gap width with increasing lattice constant by associating this effect with the particular behavior of the spin-wave amplitude profiles.

Our theoretical approach is discussed in detail in Sec. II. In the next sections we present the results of our theoretical study of the propagation of spin waves in 3D MCs based on mFT NPs arranged in sites of an fcc lattice and embedded in a ferromagnetic matrix. In Sec. III we refer to a model homogeneous medium with effective magnetic parameters to explain the characteristics of the spin-wave frequency spectra obtained for the MCs under consideration in the long-wavelength limit, that is, near the center of the Brillouin zone. Section IV presents the evolution of the magnonic band gap with the lattice constant. We also present spin-wave amplitude profiles, on the basis of which we explain the occurrence of a maximum in the lattice-constant dependence of the gap width. In Sec. V we analyze the dependence of the gap width on the matrix material. The physical grounds of the main results presented in this paper are discussed in Sec. VI. The main conclusions drawn from the results obtained in this study are summed up in Sec. VII.

II. THEORETICAL APPROACH

For the description of spin waves propagating in the magnonic crystal under consideration we are going to use a Cartesian coordinate system corresponding to regular crystal lattices, with the z axis parallel to the [001] direction in the crystal [Fig. 1(c)]. An external magnetic field homogeneous in space and strong enough to align all the magnetic moments in the direction of the field is applied along the z axis. This allows the use of the linear approximation, which implies small deviations $\mathbf{m}(\mathbf{r}, t)$ of the magnetization $\mathbf{M}(\mathbf{r}, t)$ from its ground state. Thus, the magnetization vector can be expressed as $\mathbf{M}(\mathbf{r}, t) = M_z(\mathbf{r})\hat{z} + \mathbf{m}(\mathbf{r}, t)$. Because $|\mathbf{m}(\mathbf{r}, t)| \ll M_z(\mathbf{r})$, we can assume $M_z(\mathbf{r}) \approx M_S(\mathbf{r})$, where M_S is the saturation

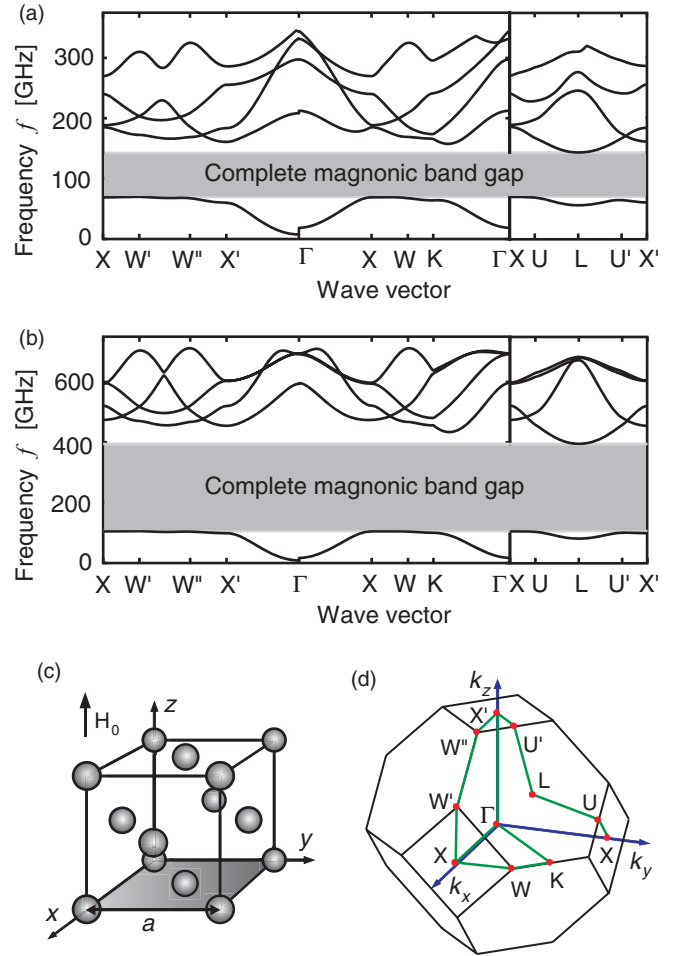


FIG. 1. (Color online) (a) and (b) Spin-wave spectra of MC with magnetoferritin (mFT) nanoparticles embedded in an iron matrix and arranged in an fcc lattice with lattice constant (a) 18.5 nm (mFT crystal as prepared) and (b) 14 nm (dehydrated mFT crystal). The spectra are plotted along the high-symmetry path in the first Brillouin zone shown in (d). Shaded area represents the complete magnonic band gap. (c) Schematic plot of the fcc structure with coordinating system used.

magnetization. In this study we will seek solutions in the form of monochromatic spin waves $\mathbf{m}(\mathbf{r}, t) = \mathbf{m}(\mathbf{r})e^{i\omega t}$, ω being the spin-wave angular frequency.

In the classical approach the dynamics of the magnetization is described by the Landau-Lifshitz (LL) equation:

$$\frac{\partial \mathbf{M}}{\partial t} = -|\gamma|\mu_0 \mathbf{M} \times \mathbf{H}_{\text{eff}}, \quad (1)$$

where γ is the gyromagnetic ratio, μ_0 is the permeability of vacuum, and \mathbf{H}_{eff} is the effective magnetic field. As in the case of free electrons, we assume $|\gamma|\mu_0 = 2.21 \times 10^5 \text{ mA}^{-1} \text{ s}^{-1}$. Damping is neglected in the calculations performed in this study.

The effective magnetic field \mathbf{H}_{eff} acting on magnetic moments in an MC is in general a sum of several components. If the magnetocrystalline anisotropy is negligible in the studied

structure \mathbf{H}_{eff} can be written as

$$\mathbf{H}_{\text{eff}}(\mathbf{r}, t) = \mathbf{H}_0 + \mathbf{H}_{\text{ex}}(\mathbf{r}, t) + \mathbf{H}_{\text{ms}}(\mathbf{r}, t). \quad (2)$$

The first component of the effective field in (2) is the applied magnetic field. The second component is the exchange field. To express this field we shall use the formula specified in Ref. 58: $\mathbf{H}_{\text{ex}}(\mathbf{r}, t) = [\nabla \lambda_{\text{ex}}^2(\mathbf{r}, t) \nabla] \mathbf{m}(\mathbf{r}, t)$, where $\lambda_{\text{ex}} = \sqrt{2A/\mu_0 M_S^2}$ is the exchange length and A is the exchange constant. The last component of the effective field is the magnetostatic field. In the linear approximation it can be decomposed into the static and dynamic components $\mathbf{H}(\mathbf{r})$ and $\mathbf{h}(\mathbf{r}, t)$, respectively, $\mathbf{H}_{\text{ms}}(\mathbf{r}, t) = \mathbf{H}(\mathbf{r}) + \mathbf{h}(\mathbf{r}, t)$, where $|\mathbf{h}(\mathbf{r}, t)| \ll |\mathbf{H}(\mathbf{r})|$. The time dependence of the dynamic component of the dipolar field has the same form as that of the dynamic component of the magnetization vector $\mathbf{h}(\mathbf{r}, t) = \mathbf{h}(\mathbf{r})e^{i\omega t}$.

The calculations of the spin-wave spectra of 3D MCs performed to date (see, e.g., Refs. 57 and 58) only take into consideration inhomogeneity of the dynamic magnetostatic field. In this study we extend our previous results by allowing for an inhomogeneous static demagnetizing field. In the linear approximation, (1) leads to the following system of equations:

$$\begin{aligned} \tilde{\omega} m_x &= -M_S [(\nabla \lambda_{\text{ex}}^2 \nabla) m_y + h_y] + (H_0 + H_z) m_y, \\ \tilde{\omega} m_y &= M_S [(\nabla \lambda_{\text{ex}}^2 \nabla) m_x + h_x] - (H_0 + H_z) m_x, \end{aligned} \quad (3)$$

where $\tilde{\omega} = i\omega/|\gamma|\mu_0$. The static demagnetizing field is assumed to have only one nonzero component H_z along the direction of the external field. The other two components H_x and H_y must be neglected for the equations to be consistent under the linear approximation used.

Let us consider an MC composed of two ferromagnetic materials, A and B. Material A is distributed periodically in the MC in the form of spherical scattering centers arranged in an fcc lattice. The spheres of material A are embedded in a matrix of material B. A periodic spatial distribution of magnetic parameters is of key importance for the magnonic properties of composites of this type. These material parameters, namely A and M_S , and consequently λ_{ex}^2 , are periodic functions of the position vector $\mathbf{r}(x, y, z)$, with the same periodicity as the lattice. Thus, we can use the Fourier transformation to map these periodic functions to the reciprocal space in the following way:

$$\begin{aligned} M_S(\mathbf{r}) &= \sum_{\mathbf{G}} M_S(\mathbf{G}) \exp(i\mathbf{G} \cdot \mathbf{r}), \\ \lambda_{\text{ex}}^2(\mathbf{r}) &= \sum_{\mathbf{G}} \lambda_{\text{ex}}^2(\mathbf{G}) \exp(i\mathbf{G} \cdot \mathbf{r}), \end{aligned} \quad (4)$$

where \mathbf{G} denotes a vector of the reciprocal lattice of the considered fcc structure. In the case of spherical scattering centers the Fourier components $M_S(\mathbf{G})$ and $\lambda_{\text{ex}}^2(\mathbf{G})$ of the saturation magnetization and the squared exchange length, respectively, can be easily obtained analytically, and have the form

$$X(\mathbf{G}) = \begin{cases} ff X_{A-B} + X_B & \text{for } \mathbf{G} = 0, \\ 3ff X_{A-B} (\sin P - P \cos P) / P^3 & \text{for } \mathbf{G} \neq 0, \end{cases} \quad (5)$$

where $X_{A-B} = (X_A - X_B)$; X stands for M_S or λ_{ex}^2 ; subscripts A and B refer to the scattering centers and the matrix, respectively; $P = R|\mathbf{G}|$, where R is the scattering center radius; ff is the filling fraction, defined as the volume proportion of material A in the unit cell. For spheres of radius R arranged in an fcc lattice with lattice constant a the filling fraction is $ff = 16\pi R^3/3a^3$.

In order to solve the system of Eqs. (3) we will use the Bloch theorem, which asserts that a solution of a differential equation with periodic coefficients can be represented as the product of a plane wave envelope function and a periodic function $\mathbf{m}_k(\mathbf{G})$:

$$\mathbf{m}(\mathbf{r}) = \sum_{\mathbf{G}} \mathbf{m}_k(\mathbf{G}) \exp[i(\mathbf{k} + \mathbf{G}) \cdot \mathbf{r}], \quad (6)$$

where \mathbf{k} is a Bloch wave vector of the spin wave.

To complete the formalism in which an eigenvalue problem in the reciprocal space is derived from the system of Eqs. (3) we need to calculate the magnetostatic field $\mathbf{H}_{\text{ms}}(\mathbf{r}, t)$. In the magnetostatic approximation both the dynamic and static components of the dipolar field must fulfill Maxwells equations:

$$\begin{aligned} \nabla \times \mathbf{H}(\mathbf{r}) &= 0, & \nabla \cdot [\mathbf{H}(\mathbf{r}) + M_S(\mathbf{r})\hat{\mathbf{z}}] &= 0, \\ \nabla \times \mathbf{h}(\mathbf{r}, t) &= 0, & \nabla \cdot [\mathbf{h}(\mathbf{r}, t) + \mathbf{m}(\mathbf{r}, t)] &= 0. \end{aligned} \quad (7)$$

According to these equations, one can introduce the magnetostatic potentials for both magnetic fields:

$$\mathbf{H}(\mathbf{r}) = -\nabla\varphi(\mathbf{r}), \quad \mathbf{h}(\mathbf{r}, t) = -\nabla\psi(\mathbf{r}, t). \quad (8)$$

By applying the Bloch theorem and Fourier expanding all the periodic functions in (7) and (8) by formulas (4)–(6) one obtains the magnetic field in the considered MC as a function of the magnetization vector:

$$\begin{aligned} h_x(\mathbf{r}) &= - \sum_{\mathbf{G}} \frac{(k_x + G_x)^2 m_{x,k}(\mathbf{G}) + (k_x + G_x)(k_y + G_y) m_{y,k}(\mathbf{G})}{|\mathbf{k} + \mathbf{G}|^2} e^{i(\mathbf{k} + \mathbf{G}) \cdot \mathbf{r}}, \\ h_y(\mathbf{r}) &= - \sum_{\mathbf{G}} \frac{(k_x + G_x)(k_y + G_y) m_{x,k}(\mathbf{G}) + (k_x + G_x)^2 m_{y,k}(\mathbf{G})}{|\mathbf{k} + \mathbf{G}|^2} e^{i(\mathbf{k} + \mathbf{G}) \cdot \mathbf{r}}, \\ H_z(\mathbf{r}) &= - \sum_{\mathbf{G}} \frac{G_z^2}{G^2} M_S(\mathbf{G}) e^{i\mathbf{G} \cdot \mathbf{r}}. \end{aligned} \quad (9)$$

Substitution of Eqs. (4), (6), and (9) into (3) leads to an eigenvalue problem with eigenvalues $\Omega = i\omega/|\gamma|\mu_0 H_0$:

$$\hat{M}\mathbf{m}_k(\mathbf{G}) = \Omega\mathbf{m}_k(\mathbf{G}), \quad (10)$$

where the eigenvector is defined as $\mathbf{m}_k = [m_{x,k}(\mathbf{G}_1), \dots, m_{x,k}(\mathbf{G}_N), m_{y,k}(\mathbf{G}_1), \dots, m_{y,k}(\mathbf{G}_N)]^T$, and a finite number N of reciprocal lattice vectors is used in (4)–(6). The block-matrix \hat{M} has the form $\hat{M} = \begin{bmatrix} \hat{M}_{xx} & \hat{M}_{xy} \\ \hat{M}_{yx} & \hat{M}_{yy} \end{bmatrix}$ with following elements:

$$\begin{aligned} M_{ij}^{xx} &= -M_{ij}^{yy} = \frac{(k_x + G_{x,i})(k_y + G_{y,j})M_S(\mathbf{G}_i - \mathbf{G}_j)}{H_0|\mathbf{k} + \mathbf{G}_j|^2}, \\ M_{ij}^{xy} &= \delta_{ij} + \frac{1}{H_0} \sum_l (\mathbf{k} + \mathbf{G}_l)(\mathbf{k} + \mathbf{G}_j)\lambda_{\text{ex}}^2(\mathbf{G}_l - \mathbf{G}_j) \\ &\quad \times M_S(\mathbf{G}_i - \mathbf{G}_l) + \frac{(k_y + G_{y,j})^2 M_S(\mathbf{G}_i - \mathbf{G}_j)}{H_0|\mathbf{k} + \mathbf{G}_j|^2} \\ &\quad - \frac{(G_{z,i} + G_{z,j})^2 M_S(\mathbf{G}_i - \mathbf{G}_j)}{H_0|\mathbf{G}_i + \mathbf{G}_j|^2}, \quad (11) \\ M_{ij}^{yx} &= -\delta_{ij} - \frac{1}{H_0} \sum_l (\mathbf{k} + \mathbf{G}_l)(\mathbf{k} + \mathbf{G}_j)\lambda_{\text{ex}}^2(\mathbf{G}_l - \mathbf{G}_j) \\ &\quad \times M_S(\mathbf{G}_i - \mathbf{G}_l) - \frac{(k_x + G_{x,j})^2 M_S(\mathbf{G}_i - \mathbf{G}_j)}{H_0|\mathbf{k} + \mathbf{G}_j|^2} \\ &\quad + \frac{(G_{z,i} + G_{z,j})^2 M_S(\mathbf{G}_i - \mathbf{G}_j)}{H_0|\mathbf{G}_i + \mathbf{G}_j|^2}, \end{aligned}$$

where indices i, j , and l are integers in the range $\langle -N, N \rangle$. We solve the eigenvalue problem (10) by standard numerical routines using 1241 plane waves or reciprocal vectors \mathbf{G} which is enough to obtain convergence of the results (with an error less than 2%) for both lowest magnonic gap width and its central frequency.

III. PROPERTIES OF THE SPIN-WAVE SPECTRUM

We have used the theoretical method discussed above to determine the spin-wave spectrum of magnonic crystals based on mFT NPs arranged in an fcc lattice and embedded in a ferromagnetic matrix. The matrix materials considered are cobalt, iron, nickel, permalloy (Py), and yttrium iron garnet (YIG). The material parameters used in the calculations are specified in Table I. In all considered cases we assume an external magnetic field of 0.1 T to stabilize the uniform magnetization in the crystal.

Figures 1(a) and 1(b) presents sample magnonic spectra obtained for an Fe matrix and two values of the lattice constant:

TABLE I. Values of material parameters: Spontaneous magnetization M_S , exchange stiffness constant A , and exchange length λ_{ex} , in the materials considered in this study (see, e.g., Ref. 84).

Material	Fe	Co	Py	Ni	YIG	mFT ^a
M_S (A/m) 10^6	1.752	1.390	0.810	0.480	0.194	0.346
A (J/m) 10^{-11}	2.1	2.8	1.1	0.86	0.4	1.0
λ_{ex} (nm)	3.30	4.80	5.17	7.71	13.01	11.53

^aParameter values calculated on the basis of Ref. 9.

18.5 nm (mFT crystal as prepared) and 14 nm (dehydrated mFT crystal), respectively. The spectra were calculated along the high-symmetry path in the first Brillouin zone (FBZ) shown in Fig. 1(d). The introduction of the iron matrix in which the mFT NPs are embedded is seen to generate a complete magnonic band gap for both lattice constant values. In the first case, $a = 18.5$ nm, the gap width is 73 GHz, and its central frequency 106 GHz [Fig. 1(a)]. For the other lattice constant value, $a = 14$ nm, the band gap has a width of 290 GHz and is centered at 250 GHz [Fig. 1(b)]. Thus, the decrease in the lattice constant by approximately 24% results in a nearly fourfold increase in the gap width and a substantially higher forbidden frequency range. Similar results were obtained for the Co matrix (gap width 79 GHz for $a = 18.5$ nm and 246 GHz for $a = 14$ nm) and the Py matrix (gap width 28 GHz for $a = 18.5$ nm and 136 GHz for $a = 14$ nm). For the Ni and YIG matrices no magnonic band gap was found to occur.

A frequency step is seen to occur at point Γ in the spin-wave spectra presented in Fig. 1. At this point the direction of propagation of the spin wave changes from parallel (segment $X'-\Gamma$) to perpendicular (segment $\Gamma-X$) with respect to the applied field. The frequency step is due to the dipolar interactions and occurs also in homogeneous materials.⁸⁵ In an infinite homogeneous medium with saturation magnetization M_S and exchange length λ_{ex} the dependence of the spin-wave frequency on the wave vector magnitude k is⁸⁵

$$\omega_\theta(k) = \sqrt{(\omega_0 + \omega_M \lambda_{\text{ex}}^2 k^2)[\omega_0 + \omega_M(\lambda_{\text{ex}}^2 k^2 + \sin^2 \theta)]}, \quad (12)$$

where $\omega_0 = |\gamma|\mu_0 H_0$ is the ferromagnetic resonance frequency in the external field H_0 , $\omega_M = |\gamma|\mu_0 M_S$, and θ is the angle between the direction of propagation of the spin wave and that of the external field. Hence, for $k = 0$, that is, at point Γ of the Brillouin zone, the reorientation of the direction of propagation from parallel to perpendicular to H_0 results in the frequency shift

$$\Delta\omega \equiv \omega_{90} - \omega_0 = \omega_0 \left(\sqrt{1 + \frac{M_S}{H_0}} - 1 \right). \quad (13)$$

If we replace the MC by a homogeneous medium the effective value of saturation magnetization (in the simplest model) can be found from the weighted mean:

$$M_S^{\text{eff}} = M_S^A ff + M_S^B (ff - 1). \quad (14)$$

For the lattice constant 18.5 nm from (13) and (14) we obtain the step $\Delta\omega/2\pi = 9.73$ GHz for the effective medium, against $\Delta\omega/2\pi = 10.95$ GHz obtained by the PWM for a magnonic crystal. For the lattice constant 14 nm the step calculated on the basis of the effective parameters is $\Delta\omega/2\pi = 8.44$ GHz, against the composite value $\Delta\omega/2\pi = 8.36$ GHz. This agreement between the numerical results obtained for a composite with a large contrast of magnetic parameters and the analytical data for a homogeneous material with effective (averaged) parameters is indicative of a highly uniform lowest mode in the long-wave end of the spin-wave spectrum. [This conclusion is confirmed by the dynamic magnetization profiles obtained by the PWM, cf. Figs. 4(a)–4(c).] However, the specific values of ω_0 and ω_{90} for the magnonic crystal are

much higher than those for the homogeneous material with averaged parameters. For example, for the lattice constant values 18.5 and 14 nm we have $\omega_0/2\pi = 7.54$ GHz and $\omega_0/2\pi = 8.48$ GHz, respectively, against $\omega_0/2\pi = 2.80$ GHz for the homogeneous medium. These differences may result from taking into account in the PWM the static demagnetizing field, which strongly depends on the lattice constant. Thus, the demagnetization effects can have a substantial impact on the spin-wave spectrum, especially in the range of small wave vectors, and should be taken into account in the model with the effective homogeneous medium, for example, by including a correction term corresponding to the effective (average) impact of the demagnetizing field⁸⁶ and correcting the value of the external field accordingly. In the cases discussed above the values of this additional magnetic field are 0.17 T for $a = 18.5$ nm and 0.2 T for $a = 14$ nm.

Another question is: Why no band gap occurs for Ni and YIG matrices? This topic is discussed in detail in Sec. VI.

IV. MAGNONIC BAND GAP VS LATTICE CONSTANT

We have also examined the lattice-constant dependence of the width of the complete magnonic band gap. The results are presented in Fig. 2(a). For spheres with a diameter of 8 nm (the diameter of the ferromagnetic core of a magnetoferritin particle) arranged in an fcc lattice the minimal lattice constant is 11.5 nm, approximately. As the lattice constant grows from this minimal value to approximately 13 nm, the gap width increases steeply, to decrease, at first very rapidly, as the lattice constant increases still further. Thus, for all the three matrix materials for which the band gap opens a pronounced maximum of the gap width occurs for a lattice constant value close to 13 nm, namely 13.02 nm for Co, 12.77 nm for Fe, and 12.82 nm for Py. The band gap proves to close at the largest lattice constant value $a_{\max} = 27$ nm in the structure with a

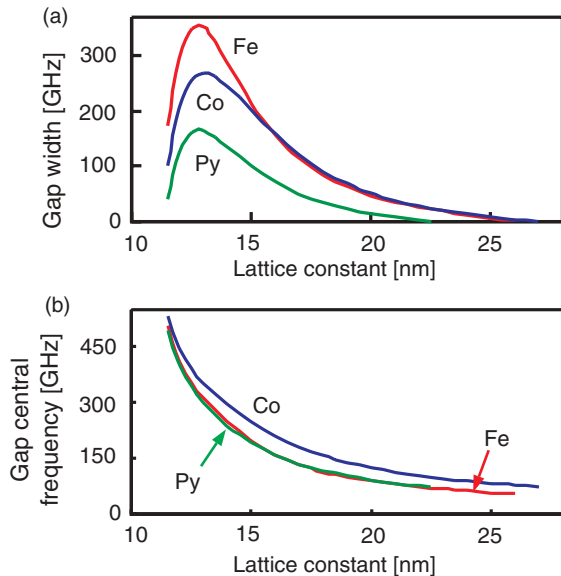


FIG. 2. (Color online) (a) The width and (b) the central frequency of the complete magnonic band gap vs lattice constant for magnetoferritin-based magnonic crystals with an iron, cobalt, and permalloy matrix.

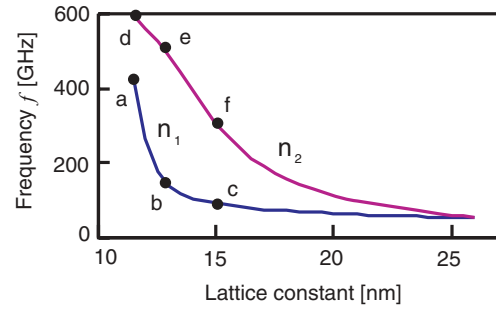


FIG. 3. (Color online) The top of the first band (n_1) and the bottom of the second band (n_2) vs the lattice constant for mFT NPs in Fe. Points a–f correspond to the dynamic magnetization profiles shown in Fig. 4.

cobalt matrix. For the iron matrix the maximal lattice constant value corresponding to a nonzero band gap is $a_{\max} = 26$ nm, and for permalloy $a_{\max} = 22.5$ nm. Figure 2(b) shows the central frequency of the complete magnonic band gap versus the lattice constant. For Fe and Py matrices the central frequencies are nearly equal, only differing by a few percent. For cobalt the central frequency is substantially higher. In all three cases the gap center lowers monotonically as the lattice constant grows. These dependencies offer a way to model the complete magnonic band gap in a wide range.

Let us explain the occurrence of a maximum in the lattice-constant dependence of the gap width. This maximum is related to changes in the character of the dynamic magnetization profile for the two lowest modes at points L and W' in the FBZ, corresponding to the wave vectors for which these modes delimit the band gap. Figure 3 shows the top of the first band (the bottom of the magnonic band gap) and the bottom of the second band (the top of the band gap) versus the lattice constant for mFT NPs embedded in Fe. In the lattice constant range from 11.5 to approximately 13 nm the top of the first band (n_1) drops very rapidly. The bottom frequency of the second band (n_2) decreases as well, but at a much slower rate. As a result the band gap widens. For the lattice constant of approximately 13 nm the slope of both curves is significantly different. First of all, the frequency of the lowest mode diminishes much more slowly than that of the second mode, which results in a shrinkage of the band gap.

To explain this behavior of the two lowest modes we determined their spin-wave profiles (dynamic magnetization profiles) for three lattice constant values, indicated in the plot shown in Fig. 3 (points a–f). The profiles are presented in Fig. 4. We also introduced a *concentration coefficient* of the dynamic component of magnetization. For scattering centers the concentration coefficient is defined:

$$C_A = \frac{\tilde{m}_A}{\tilde{m}_A + \tilde{m}_B}, \quad (15)$$

where $\tilde{m}_X = \frac{1}{V_X} \int_{V_X} |\mathbf{m}|^2 dv$ is the mean value of squared amplitude of the dynamic magnetization in volume V_X , that is, in the scattering centers (for $X = A$) or in the matrix ($X = B$). By this definition a concentration coefficient value above 0.5 means that the concentration of dynamic magnetization is higher in the mFT NPs than in the matrix.

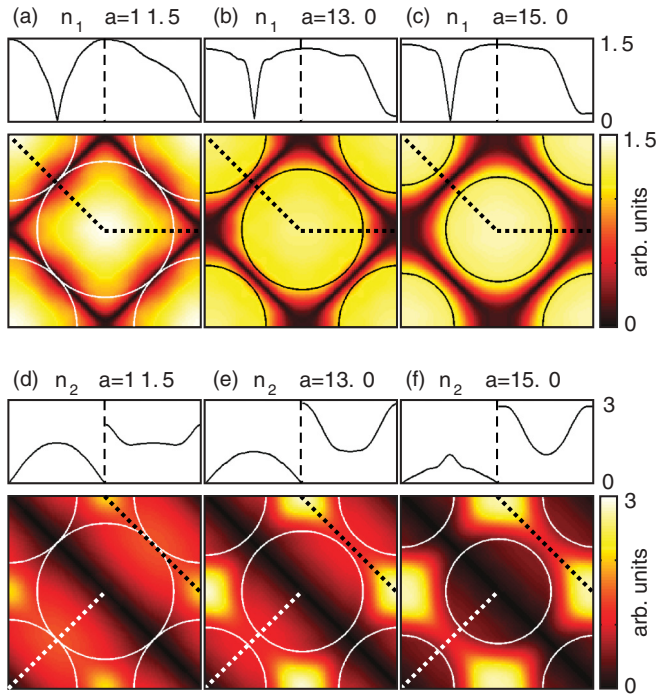


FIG. 4. (Color online) Profiles of dynamic magnetization for the two lowest spin-wave modes (n_1 and n_2) in an mFT/Fe MC in a plane perpendicular to the external field and passing through the centers of mFT NPs (the contours of which are represented by circles). Profiles labeled a–f correspond to the respective points indicated in Fig. 3. Section along the dotted lines is shown above each profile.

For the lowest mode [Figs. 4(a)–4(c)] the dynamic magnetization determined at point W' of the FBZ is strongly concentrated in the mFT NPs and the lattice-constant dependence of the concentration coefficient is very weak ($C_A = 0.69$ for $a = 11.5$ nm, 0.70 for 13 nm, and 0.73 for 15 nm). In the case of touching mFT NPs [Fig. 4(a)] the profile has a bulk character (a sinusoidal shape), manifest along the path between adjacent mFT NPs. This is due to strong interactions between excitations concentrated in adjacent NPs. An increase in the lattice constant to 13 nm brings about significant changes in the profile of the lowest mode, which becomes flat in the NPs and vanishes rapidly in the matrix [Fig. 4(b)]. This is because the role of the exchange interactions between adjacent NPs, strongly dependent on the interparticle distance, diminishes. As a result the excitations are strongly isolated and limited to the NPs. A further increase in the lattice constant does not change the character of the profiles [Fig. 4(c)], but only strengthens the isolation of the excitations in the NPs. Since also the size of the NPs remains unchanged, the excitations are concentrated in the same volume regardless of the lattice constant. Thus, the frequency of the lowest mode only depends on the lattice constant by the magnetostatic interactions between excitations in adjacent NPs; for sufficiently large lattice constant values this dependence is weak.

The profiles of the second mode [Figs. 4(d)–4(f)] were determined at point L in the FBZ, or for the direction of propagation $[111]$. This is reflected in the general shape of the profiles: Node planes, passing through NP centers, and planes of strong concentration of dynamic magnetization

alternate perpendicularly to the direction of propagation. For all three lattice constant values the dynamic magnetization is mainly concentrated in the matrix, with a maximum in the middle of interparticle areas. In this case, however, for small lattice constants ($a = 11.5$ nm), also in the NPs the amplitude of dynamic magnetization is significantly different from zero [$C_A = 0.38$, Fig. 4(d)]. As the lattice constant increases to 13 nm the dynamic magnetization leaves the NPs for the matrix ($C_A = 0.23$), which implies its increased concentration in the matrix material [Fig. 4(e)]. This increase in the concentration of dynamic magnetization in the relatively small interparticle space compensates to some extent the rapid decrease in the spin-wave frequency with growing lattice constant. This effect is manifest in the behavior of n_2 in Fig. 3 for lattice constant values between 11.5 and 13 nm. For lattice constants above 13 nm the dynamic magnetization is concentrated almost solely in the matrix ($C_A = 0.08$ for $a = 15$ nm). Further increase in the lattice constant does not result in significant changes in the character of the spin-wave profile; only the volume of matrix material, in which the dynamic magnetization is concentrated, grows with lattice constant in this range [Fig. 4(f)]. The increase in volume available for the considered excitation results directly from the change in filling fraction, as reflected in the character of the n_2 curve in Fig. 3 for lattice constant values above 13 nm.

V. MAGNONIC BAND GAP VS MATRIX MATERIAL

In the lattice constant range from 11.5 to 15 nm the largest band gap occurs for the iron matrix; the gap is much narrower for the cobalt matrix, and the narrowest for the permalloy matrix (in the lattice constant range above 15 nm the band gap width for Co is similar to that for Fe). In this range of lattice constant the distance between the centers of adjacent mFT NPs ranges from 8.1 to 10.6 nm and the exchange interactions predominate.

The values of material parameters: The saturation magnetization M_S , the exchange constant A , and the exchange length λ_{ex} , in the materials considered in this paper, are specified in Table I. Figure 5 visualizes the contrasts of these parameters,

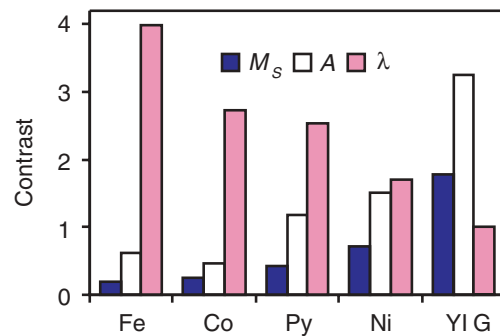


FIG. 5. (Color online) Contrast of saturation magnetization M_S , exchange constant A , and exchange length λ in magnonic crystals with mFT NPs and different matrix materials. The contrast of each parameter is the ratio of its value in the NPs to its value in the matrix material. The plotted values are as calculated on the basis of Table I. The matrix materials are ordered by decreasing gap width (except for the last two, for which the band gap does not occur).

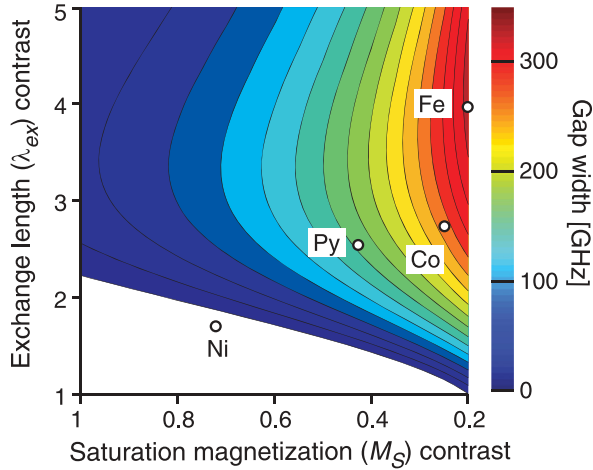


FIG. 6. (Color online) Color map of the complete magnonic band gap width vs material parameter contrasts for a magnetoferritin-based magnonic crystal with the lattice constant $a = 13.0$ nm. The material parameter values in the scattering centers (mFT) are fixed. The contrast of each parameter is the ratio of its value in the scattering centers to its value in the matrix (Table I). Open circles indicate points corresponding to the matrix materials considered in this study.

that is, the ratio of the parameter value in mFT to its value in the matrix. The matrix materials are ordered by decreasing gap width (except for the last two, for which the band gap does not occur). The M_S contrast grows monotonically with decreasing gap width; moreover, its inverse is, in a good approximation, proportional to the gap width (for the lattice constant of 13 nm, corresponding to the maximum gap width, the product of the M_S contrast and the gap width in GHz is 69.5 for Fe, 67.2 for Co, and 70.2 for Py). Also the exchange length contrast varies monotonically with the gap width; however, the difference between the values of λ_{ex} contrast for Co and Py is slight, while the gap widths for these two matrix materials differ significantly.

The occurrence of a critical material parameter contrast value to be reached for a complete magnonic gap to open is clearly seen in Fig. 6, showing a color map of the complete magnonic band gap width vs the contrasts of saturation magnetization and exchange length. The lattice constant is 13 nm and the material parameters of the mFT NPs are fixed. The contrast of each parameter is calculated as the ratio of its value in the scattering centers (mFT) to its matrix value (see Table I). The graph corresponds to a situation in which the saturation magnetization is higher in the matrix than in the NPs (the contrast value is below 1) while the exchange length is lower in the NPs than in the matrix; this occurs in MCs with four matrix materials considered in this paper: Co, Fe, Py, and Ni (marked with open circles). No complete magnonic gap will occur if both contrasts are too weak (too close to 1). The corresponding region is shown as white in Fig. 6; the MC with a nickel matrix is seen to lie in this region.

This result is similar to the data reported in Ref. 57. In Fig. 7 in this reference paper the critical value of saturation magnetization contrast, below which the band gap does not occur, is 2.8 for the fcc lattice.⁸⁷ This value was obtained for the situation in which the saturation magnetization in the matrix material is lower than in the scattering centers. In the case of

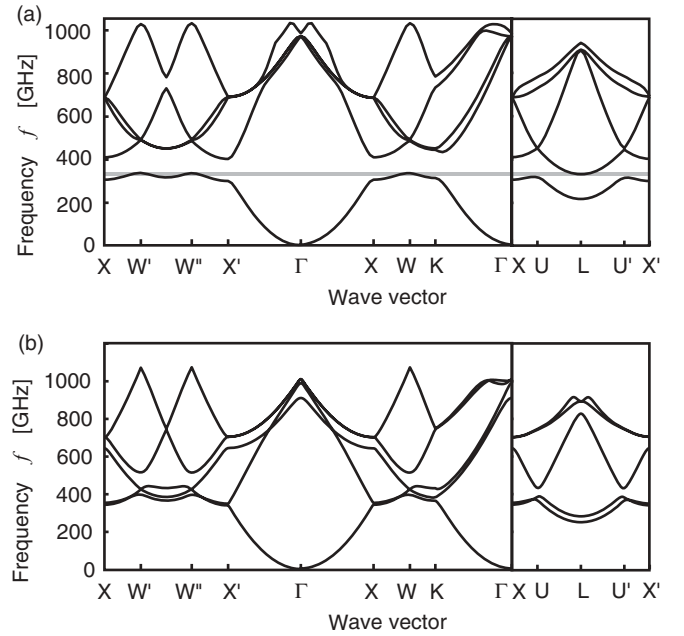


FIG. 7. Spin-wave spectra of MC with magnetoferritin (mFT) nanoparticles arranged in an fcc lattice with lattice constant 13.0 nm and embedded in an (a) nickel and (b) YIG matrix. The spectra are plotted along the high-symmetry path in the FBZ shown in Fig. 1(d). Shaded area in (a) represents overlapping of two lowest bands.

the mFT NPs considered in our study this situation only occurs for the YIG matrix; the corresponding M_S contrast is 1.78. For the other matrix materials the situation is reversed, that is, this contrast is lower than 1. Qualitatively, the conclusion is exactly as in Ref. 57: In the range of predominating exchange interactions the width of the magnonic band gap grows with increasing M_S contrast above some threshold that must be reached for the band gap to open.

This interpretation, relating the gap width with the saturation magnetization contrast, does not apply to the lattice constant range above 15 nm. The band gaps obtained for the iron and cobalt matrices are of almost equal width in this lattice-constant range; the band gap obtained for Co is slightly larger [Fig. 2(a)].

VI. DISCUSSION

Two fundamental questions arise in relation to the results presented above. What is the origin of the contrast threshold? Is it by coincidence, or rather because of an intrinsic property of the considered structures that for every three matrix materials in which the band gap opens its maximum occurs around the lattice constant of 13 nm? In an attempt to answer these questions let us remember the basic results obtained for 1D MCs.⁸⁸ There is no critical magnetic contrast in this case: Any contrast will result in a gap in the spin-wave spectrum at the border of the FBZ. In the 3D case a similar effect is observed for any particular direction of spin-wave propagation; however, in general, the FBZ border for different directions stands for different lengths of the wave vector. This results in an indirect band gap, whose bottom and top correspond to different lattice

directions. Moreover, if the directional gaps are too narrow, the overlapping of neighboring bands can destroy a complete magnonic gap. A perfect example of such a situation is the spectrum obtained for the Ni matrix, shown in Fig. 7(a). The general shape of this spectrum is similar to that obtained for the Fe matrix [cf. Fig. 1(b)], except for the fact that in the case of Ni the distance between the first and second bands is much smaller. Because of this close vicinity a frequency margin at the top of the first band overlaps with the bottom frequencies of the second band around the point L . The contrast of saturation magnetization is 0.72 in this MC, much smaller (i.e., closer to 1) than in the three cases in which a complete gap occurs. This is indicative of a certain threshold to be surpassed for the two lowest bands to disjoin and a complete magnonic gap to open. A similar rule was found in photonic crystals, in which the opening of a complete photonic gap necessitates a dielectric constant contrast above some critical value.⁸⁹

Shown in Fig. 7(b), the spin-wave spectrum obtained for the YIG matrix is substantially different from the spectra for Ni or Fe matrices; the difference is the overlapping of the two lowest bands. According to Fig. 5, only for YIG the saturation magnetization contrast is greater than one, that is, M_S in the matrix is lower than in the scattering centers. As a consequence the lowest modes are concentrated in the matrix. The concentration coefficient (15) for the matrix material, calculated at different points in the FBZ, varies from 0.51 to 0.74 for the lowest mode and from 0.58 to 0.76 for the second one. It is this concentration of two neighboring modes in the same material that allows their crossing and, consequently, prevents the opening of the band gap between them. Similar cases are studied in Ref. 57, which considers MCs with a magnetization contrast greater than 1; a complete magnonic gap is found to open above a certain level of this contrast. In the case of an fcc lattice with a lattice constant of 10 nm and a filling fraction of 0.2 the critical value of magnetization contrast is found to be 2.8. In the case considered here, with mFT NPs in a YIG matrix, the M_S contrast is 1.784. Thus, our result agrees with the findings presented in Ref. 57.

One more conclusion can be drawn from the above discussion. In all the cases with a magnetization contrast lower than 1 (i.e., with Fe, Co, Py, and Ni matrices) the magnonic band gap has a lower bound (the top of the first band) at the point W' , which is the limit of the FBZ for the direction [201], and an upper bound (the bottom of the second band) at the point L , the FBZ limit for the direction [111]. A common characteristic of these two points at the boundary of the FBZ is an extreme distance from its center: L is the closest, and W' is the farthest.⁹⁰ Hence we conclude that in the case of an indirect band gap a minimized difference between the longest and shortest wave vectors at the boundary of the FBZ is conducive to the opening of a band gap. This reasoning explains well the numerical results reported in Ref. 57, where the largest complete magnonic band gap is obtained for the fcc lattice, and the narrowest one for the sc structure. In the fcc structure the difference in the distance of the extreme FBZ boundary points from the zone center is the smallest (as small as $0.504 \pi/a$). For the bcc lattice the difference is $0.586 \pi/a$, and for the sc structure has the highest value of $0.732 \pi/a$.

Let us get back to the 1D case. If the contrast of material parameters is small it can be regarded as a perturbation. In this case the maximal value of the gap width occurs for the filling fraction $ff = 0.5$. This would apply also to the 3D case if the FBZ had a spherical shape. For an fcc lattice of mFT NPs of the radius of 4 nm the filling fraction of 0.5 corresponds to the lattice constant of 12.896 nm, pretty close to our results for the Co, Fe, and Py matrices. Since in the considered material compositions the contrasts are rather large and the FBZ of the fcc lattice is not spherical, such a good agreement might be due to a counterbalance of effects of different factors. Full elucidation of this issue requires extensive research and the consideration of a wide range of material parameters, which goes far beyond the main topic of this paper.

VII. CONCLUSIONS

In this paper we have presented the results of our theoretical study of the spin-wave spectrum of 3D magnonic crystals based on magnetoferritin nanoparticles arranged in an fcc lattice. As demonstrated by our results, the introduction of a ferromagnetic matrix filling in the interparticle space may lead to the opening of a complete band gap in the magnonic spectrum. As indicated by our findings, cobalt, iron, and permalloy should be of use as matrix materials in magnetoferritin-based magnonic crystals with well defined band gap in the spin-wave spectrum.

Another very important factor in the modeling of a magnonic band gap is the lattice constant. In the crystals considered in this study the gap width as a function of the lattice constant has a maximum for a lattice constant of approximately 13 nm. The occurrence of this maximum is related to the character of the lattice-constant evolution of the dynamic magnetization profiles for the lowest excitations in the spin-wave spectrum. Also, for lattice constants of ten-odd nanometers both the width of the band gap and its central frequency change very rapidly. On the one hand, this opens the prospect of producing 3D magnonic crystals with an intentionally modeled band gap; on the other hand, the methods of magnonic crystal production must meet higher requirements in terms of tuning the lattice constant to allow such modeling of the band gap. Our considerations lead us also to conclude that among the cubic structures the fcc lattice provide the best conditions for the occurrence of a magnonic band gap.

In light of the results presented above we conclude that dehydrated magnetoferritin-based crystals produced by the protein crystallization technique have both the crystal structure and the lattice constant close to optimal for the occurrence of a magnonic band gap.

ACKNOWLEDGMENTS

The authors would like to acknowledge valuable comments made by Professor Walther Schwarzacher from University of Bristol. The research leading to these results has received funding from the European Communitys Seventh Framework Programme (FP7/2007-2013) under Grant Agreement No. 233552 for the MAGNONICS project.

*mamica@amu.edu.pl

- ¹S. Singamaneni, V. N. Bliznyuk, Ch. Binek, and E. Y. Tsymlal, *J. Mater. Chem.* **21**, 16819 (2011).
- ²I. Yamashita, K. Iwahori, and S. Kumagai, *Biochim. Biophys. Acta* **1800**, 846 (2010).
- ³B. Sana, E. Johnson, K. Sheah, Ch. L. Poh, and S. Lim, *Biointerphases* **5**, FA48 (2010).
- ⁴M. Uchida, M. L. Flenniken, M. Allen, D. A. Willits, B. E. Crowley, S. Brumfield, A. F. Willis, L. Jackiw, M. Jutila, M. J. Young, and T. Douglas, *J. Am. Chem. Soc.* **128**, 16626 (2006).
- ⁵J. Sarkar, S. Tang, D. Shahrjerdi, and S. K. Banerjee, *Appl. Phys. Lett.* **90**, 103512 (2007).
- ⁶K. T. Nam, R. Wartena, P. J. Yoo, F. W. Liao, Y. J. Lee, Y. M. Chiang, P. T. Hammond, and A. M. Belcher, *Proc. Natl. Acad. Sci. USA* **105**, 17227 (2008).
- ⁷S. Kumagai, T. Ono, S. Yoshii, A. Kadotani, R. Tsukamoto, K. Nishio, M. Okuda, and I. Yamashita, *Appl. Phys. Express* **3**, 015101 (2010).
- ⁸L. Feng and S. Damodaran, *Thin Solid Films* **365**, 99 (2000).
- ⁹O. Kasyutich, A. Sarua, and W. Schwarzacher, *J. Phys. D* **41**, 134022 (2008).
- ¹⁰M. A. Kostianen, O. Kasyutich, J. J. L. M. Cornelissen, and R. J. M. Nolte, *Nat. Chem.* **2**, 394 (2010).
- ¹¹M. A. Kostianen, P. Ceci, M. Fornara, P. Hiekkataipale, O. Kasyutich, R. J. M. Nolte, J. J. L. M. Cornelissen, R. D. Desautels, and J. van Lieropand, *ACS Nano* **5**, 6394 (2011).
- ¹²S. A. Majetich, T. Wen, and R. A. Booth, *ACS Nano* **5**, 6081 (2011).
- ¹³S. C. Andrews, *Biochim. Biophys. Acta* **1800**, 691 (2010).
- ¹⁴M. Bozzi, G. Mignogna, S. Stefanini, D. Barra, C. Longhi, P. Valenti, and E. Chiancone, *J. Biol. Chem.* **272**, 3259 (1997).
- ¹⁵R. A. Grant, D. J. Filman, S. E. Finkel, R. Kolter, and J. M. Hogle, *Nat. Struct. Biol.* **5**, 294 (1998).
- ¹⁶C. K. Y. Fong and G. D. Hsiung, *Infect. Immun.* **6**, 865 (1972).
- ¹⁷T. Douglas and M. Young, *Adv. Mater.* **11**, 679 (1999).
- ¹⁸M. T. Klem, M. Young, and T. Douglas, *Mater. Today* **8**, 28 (2005).
- ¹⁹M. L. Flenniken, M. Uchida, L. O. Liepold, S. Kang, M. J. Young, and T. Douglas, *Curr. Top. Microbiol. Immunol.* **327**, 71 (2009).
- ²⁰M. Uchida, S. Kang, C. Reichhardt, K. Harlen, and T. Douglas, *Biochim. Biophys. Acta* **1800**, 834 (2010).
- ²¹P. M. Harrison and P. Arosio, *Biochim. Biophys. Acta* **1275**, 161 (1996).
- ²²F. C. Meldrum, V. J. Wade, D. L. Nimmo, B. R. Heywood, and S. Mann, *Nature (London)* **349**, 684 (1991).
- ²³S. Mann, *Nature (London)* **365**, 499 (1993).
- ²⁴D. P. E. Dickson, *J. Magn. Magn. Mater.* **203**, 46 (1999).
- ²⁵F. C. Meldrum, B. R. Heywood, and S. Mann, *Science* **257**, 522 (1992).
- ²⁶P. Southern, A. P. Robinson, O. I. Kasyutich, B. Warne, A. Bewick, and W. Schwarzacher, *J. Phys.: Condens. Matter* **19**, 456204 (2007).
- ²⁷O. Kasyutich, D. Tatchev, A. Hoell, F. Ogrin, C. Dewhurst, and W. Schwarzacher, *J. Appl. Phys.* **105**, 07B528 (2009).
- ²⁸M. Koralewski, J. W. Klos, M. Baranowski, Z. Mitróová, P. Kopčanský, L. Melníková, M. Okuda, and W. Schwarzacher, *Nanotechnology* **23**, 355704 (2012).
- ²⁹J. O. Vasseur, L. Dobrzynski, B. Djafari-Rouhani, and H. Puszkarski, *Phys. Rev. B* **54**, 1043 (1996).
- ³⁰H. Puszkarski and M. Krawczyk, *Solid State Phenom.* **94**, 125 (2003).
- ³¹S. A. Nikitov, Ph. Tailhades, and C. S. Tsai, *J. Magn. Magn. Mater.* **236**, 320 (2001).
- ³²V. V. Kruglyak, S. O. Demokritov, and D. Grundler, *J. Phys. D* **43**, 264001 (2010).
- ³³B. Lenk, H. Ulrichs, F. Garbs, and M. Münzenberg, *Phys. Rep.* **507**, 107 (2011).
- ³⁴S. Neusser and D. Grundler, *Adv. Mater.* **21**, 2927 (2009).
- ³⁵A. A. Serga, A. V. Chumak, and B. Hillebrands, *J. Phys. D* **43**, 264002 (2010).
- ³⁶V. V. Kruglyak and R. J. Hicken, *J. Magn. Magn. Mater.* **306**, 191 (2006).
- ³⁷K.-S. Lee and S.-K. Kim, *J. Appl. Phys.* **104**, 053909 (2008).
- ³⁸T. Schneider, A. A. Serga, B. Leven, and B. Hillebrands, R. L. Stamps, and M. P. Kostylev, *Appl. Phys. Lett.* **92**, 022505 (2008).
- ³⁹F. Macia, A. D. Kent, and F. C. Hoppensteadt, *Nanotechnology* **22**, 095301 (2011).
- ⁴⁰A. Khitun, M. Bao, and K. L. Wang, *J. Phys. D* **43**, 264005 (2010).
- ⁴¹R. V. Mikhaylovskiy, E. Hendry, and V. V. Kruglyak, *Phys. Rev. B* **82**, 195446 (2010).
- ⁴²A. V. Butko, A. A. Klimov, S. A. Nikitov, and Yu. A. Filimonov, *J. Commun. Technol. Electron.* **51**, 944 (2006).
- ⁴³S. L. Vysotskii, S. A. Nikitov, and Yu. A. Filimonov, *JETP* **101**, 547 (2005).
- ⁴⁴M. Kostylev, G. Gubbiotti, G. Carlotti, G. Socino, S. Tacchi, C. Wang, N. Singh, A. O. Adeyeye, and R. L. Stamps, *J. Appl. Phys.* **13**, 07C507 (2008).
- ⁴⁵S. Neusser, B. Botters, M. Becherer, D. Schmitt-Landsiedel, and D. Grundler, *Appl. Phys. Lett.* **93**, 122501 (2008).
- ⁴⁶V. V. Kruglyak, P. S. Keatley, A. Neudert, R. J. Hicken, J. R. Childress, and J. A. Katine, *Phys. Rev. Lett.* **104**, 027201 (2010).
- ⁴⁷R. Zivieri, F. Montoncello, L. Giovannini, F. Nizzoli, S. Tacchi, M. Madami, G. Gubbiotti, G. Carlotti, and A. O. Adeyeye, *Phys. Rev. B* **83**, 054431 (2011).
- ⁴⁸G. Gubbiotti, S. Tacchi, M. Madami, G. Carlotti, A. O. Adeyeye, and M. Kostylev, *J. Phys. D* **43**, 264003 (2010).
- ⁴⁹S. Tacchi, M. Madami, G. Gubbiotti, G. Carlotti, H. Tanigawa, T. Ono, and M. P. Kostylev, *Phys. Rev. B* **82**, 024401 (2010).
- ⁵⁰Z. K. Wang, V. L. Zhang, H. S. Lim, S. C. Ng, M. H. Kuok, S. Jain, and A. O. Adeyeye, *Appl. Phys. Lett.* **94**, 083112 (2009).
- ⁵¹Z. K. Wang, V. L. Zhang, H. S. Lim, S. C. Ng, M. H. Kuok, S. Jain, and A. O. Adeyeye, *ACS Nano* **4**, 643 (2010).
- ⁵²S. Tacchi, G. Duerr, J. W. Klos, M. Madami, S. Neusser, G. Gubbiotti, G. Carlotti, M. Krawczyk, and D. Grundler, *Phys. Rev. Lett.* **109**, 137202 (2012).
- ⁵³M. Krawczyk and H. Puszkarski, *Acta Phys. Pol. A* **93**, 805 (1998).
- ⁵⁴E. Tartakovskaya, W. Kreuzpaintner, and A. Schreyer, *J. Appl. Phys.* **103**, 023913 (2008).
- ⁵⁵M. Krawczyk and H. Puszkarski, *Cryst. Res. Technol.* **41**, 547 (2006).
- ⁵⁶M. Krawczyk and H. Puszkarski, *J. Appl. Phys.* **100**, 073905 (2006).
- ⁵⁷M. Krawczyk and H. Puszkarski, *Phys. Rev. B* **77**, 054437 (2008).
- ⁵⁸M. Krawczyk, J. Klos, M. L. Sokolovskyy, and S. Mamica, *J. Appl. Phys.* **108**, 093909 (2010).
- ⁵⁹S. Mamica, M. Krawczyk, and J. W. Klos, *Adv. Cond. Mat. Phys.* **2012**, 161387 (2012).
- ⁶⁰R. Arias and D. L. Mills, *Phys. Rev. B* **63**, 134439 (2001).
- ⁶¹R. Arias and D. L. Mills, *Phys. Rev. B* **70**, 094414 (2004).
- ⁶²L. Giovannini, F. Montoncello, and F. Nizzoli, *Phys. Rev. B* **75**, 024416 (2007).

- ⁶³R. Zivieri, F. Montoncello, L. Giovannini, F. Nizzoli, S. Tacchi, M. Madami, G. Gubbiotti, G. Carlotti, and A. O. Adeyeye, *IEEE Trans. Magn.* **47**, 1563 (2011).
- ⁶⁴S. Tacchi, F. Montoncello, M. Madami, G. Gubbiotti, G. Carlotti, L. Giovannini, R. Zivieri, F. Nizzoli, S. Jain, A. O. Adeyeye, and N. Singh, *Phys. Rev. Lett.* **107**, 127204 (2011).
- ⁶⁵Y. V. Gulyaev, S. A. Nikitov, and A. I. Volkov, *J. Commun. Technol. Electron.* **50**, 1024 (2005).
- ⁶⁶P. V. Bondarenko, A. Yu. Galkin, B. A. Ivanov, and C. E. Zaspel, *Phys. Rev. B* **81**, 224415 (2010).
- ⁶⁷K. M. Lebecki, M. J. Donahue, and M. W. Gutowski, *J. Phys. D* **41**, 175005 (2008).
- ⁶⁸C. C. Dantas and L. A. de Andrade, *Phys. Rev. B* **78**, 024441 (2008).
- ⁶⁹S. Neusser, B. Botters, and D. Grundler, *Phys. Rev. B* **78**, 054406 (2008).
- ⁷⁰M. Dvornik and V. V. Kruglyak, *Phys. Rev. B* **84**, 140405(R) (2011).
- ⁷¹D. Kumar, O. Dmytriiev, S. Ponraj, and A. Barman, *J. Phys. D* **45**, 015001 (2012).
- ⁷²J. D. Joannopoulos, R. D. Meade, and J. N. Winn, *Photonic Crystals: Molding the Flow of Light* (Princeton University Press, Princeton, 2008).
- ⁷³D. W. Prather, S. Shi, A. Sharkawy, J. Murakowski, and G. J. Schneider, *Photonic Crystals: Theory, Applications, and Fabrication* (Wiley, New York, 2009).
- ⁷⁴J. O. Vasseur, P. A. Deymier, B. Djafari-Rouhani, Y. Pennec, and A.-C. Hladky-Hennion, *Phys. Rev. B* **77**, 085415 (2008).
- ⁷⁵V. Laude, M. Wilm, S. Benchabane, and A. Khelif, *Phys. Rev. E* **71**, 036607 (2005).
- ⁷⁶R. P. Tiwari and D. Stroud, *Phys. Rev. B* **81**, 220403 (2010).
- ⁷⁷A. Raman and S. Fan, *Phys. Rev. Lett.* **104**, 087401 (2010).
- ⁷⁸M. L. Sokolovskyy and M. Krawczyk, *J. Nanopart. Res.* **13**, 6085 (2011).
- ⁷⁹J. W. Kłos, M. Krawczyk, and M. L. Sokolovskyy, *J. Appl. Phys.* **109**, 07D311 (2011).
- ⁸⁰S. Neusser, G. Duerr, S. Tacchi, M. Madami, M. L. Sokolovskyy, G. Gubbiotti, M. Krawczyk, and D. Grundler, *Phys. Rev. B* **84**, 094454 (2011).
- ⁸¹S. Neusser, H. G. Bauer, G. Duerr, R. Huber, S. Mamica, G. Woltersdorf, M. Krawczyk, C. H. Back, and D. Grundler, *Phys. Rev. B* **84**, 184411 (2011).
- ⁸²H. Yang, G. Yun, and Y. Cao, *J. Appl. Phys.* **111**, 013908 (2012).
- ⁸³G. Biotteau, M. Hennion, F. Moussa, J. Rodriguez-Carvajal, L. Pinsard, A. Revcolevschi, Y. M. Mukovskii, and D. Shulyatev, *Phys. Rev. B* **64**, 104421 (2001).
- ⁸⁴M. Krawczyk and H. Puzkarski, *Acta Phys. Superficerum* **3**, 89 (1999).
- ⁸⁵D. D. Stancil and A. Prabhakar, *Spin Waves. Theory and Applications* (Springer, New York, 2009).
- ⁸⁶R. Zivieri, S. Tacchi, F. Montoncello, L. Giovannini, F. Nizzoli, M. Madami, G. Gubbiotti, G. Carlotti, S. Neusser, G. Duerr, and D. Grundler, *Phys. Rev. B* **85**, 012403 (2012).
- ⁸⁷In the text of Ref. 57 the value of 2.8 is attributed to the sc lattice, and 4.8 to the fcc lattice; however, this is a clear reversal of the results presented in Fig. 7 of the same paper. Both our study and the other results reported in Ref. 57 lead to the conclusion that the opening of a complete magnonic band gap is the easiest in the fcc structure, and the most difficult in the sc structure (cf. the discussion in Sec. III).
- ⁸⁸M. Krawczyk, J.-C. Lévy, D. Mercier, and H. Puzkarski, *Phys. Lett. A* **282**, 186 (2001).
- ⁸⁹See, e.g., Ref. 72, p. 251.
- ⁹⁰Actually, points W , W' , and W'' are equidistant from the center; however, they are not equivalent because of the external field; the lowest band has a maximum at point W' .